11 Mar 2020

Interfacial Shear Bond Strength between Steel H-piles and Polymer Concrete Jackets

Mohanad M. Abdulazeez

Kyle Brown

Mohamed ElGawady
Missouri University of Science and Technology, elgawadym@mst.edu

Recommended Citation

M. M. Abdulazeez et al., "Interfacial Shear Bond Strength between Steel H-piles and Polymer Concrete Jackets," *Transportation Research Record (TRR): Journal of the Transportation Research Board*, National Academy of Sciences: Transportation Research Board, Mar 2020.
The definitive version is available at https://doi.org/10.1177/0361198120909837

TRR
JOURNAL OF THE TRANSPORTATION RESEARCH BOARD

Research Article

Transportation Research Record
1–11

DOI: 10.1177/0361198120909837
journals.sagepub.com/home/trr
SAGE

Interfacial Shear Bond Strength between Steel H-Piles and Polymer Concrete Jackets

Mohanad M. Abdulazeez[1], Kyle Brown[1], and Mohamed A. ElGawady[1]

Abstract

Steel H-piles have been used widely in bridge construction throughout the U.S. because of their relatively large load-carrying capacity while occupying a small area. However, many H-piles suffer from corrosion, which may lead to abrupt collapse. A cost-effective repair technique, including encasing the corroded region of the steel pile into a concrete jacket, which acts as an alternative load path for the applied axial load, has been used by several state Departments of Transportation. Methyl methacrylate polymer concrete (MMA-PC) is a type of concrete that is commonly used as a repair material. However, there is limited research on the assessment of bond strength between MMA-PC and steel elements. This paper investigates experimentally the bond behavior of seven full-scale steel H-piles encased in concrete jackets. The jackets were cast using either MMA-PC or Portland cement concrete (CC). Different embedment lengths of 63.5 mm (2.5 in.), 127 mm (5 in.), and 190.5 mm (7.5 in.) were used for the MMA-PC and one embedment length of 254 mm (10 in.) was used for the CC jacket. Cylindrical and prismatic jacket configurations were used and tested using push-out. The experimental results revealed that using the MMA-PC jacket was more effective compared with the CC jacket in relation to the load-carrying capacity. For design purposes, a shear bond stress of 2.96 MPa [0.43 kips per square inch (ksi)] can be used for MMA-PC jackets having an embedment length of at least 127 mm (5 in.) whereas a value of 0.83 MPa (0.12 ksi) can be used for CC.

Steel H-piles have been used widely in bridge construction throughout the U.S. because of their relatively large load-carrying capacity while occupying a small area. As a result of their exposure to repeated wetting and drying cycles throughout their service life, many H-piles suffer from corrosion, which impairs their structural integrity, capacity, and serviceability and can lead to abrupt collapses (*1–4*).

Various repair techniques such as fiber-reinforced polymer jacket (*5–7*), concrete-filled pultruded fiber-reinforced polymer tubes (*8*), and steel plates (*9*) have been used by many Departments of Transportation (DOTs) in the U.S. to restore the carrying capacity of corroded piles, based on the level of corrosion and targeted performance objective of the corroded piles. Another cost-effective repair technique is concrete encasement, in which the corroded region of the steel pile is encased in a concrete jacket (*10*, *11*).

For severely corroded H-piles, the concrete jacket works as an alternative load path for the applied axial load. Therefore, the concrete jacket needs to extend an embedment length beyond the corroded section (*11*). The required concrete embedment length depends on the shear bond strength between the concrete and embedded steel pile. A proper assessment of the shear bond strength between the concrete and steel is, therefore, crucial for the repair of corroded steel pile.

There is only a single study that investigated the shear bond strength between Portland cement-based concrete (hereinafter called conventional concrete or CC) and steel piles (*11*). The investigation was carried out using push-out tests on full-scale steel piles encased in concrete and found that the shear bond strength ranged from 0.56 MPa [0.08 kips per square inch (ksi)] to 0.83 MPa (0.12 ksi). Two studies in the literature were conducted to determine the shear bond strength between steel H-pile sections and CC using a push-out test (*12*, *13*). Different parameters such as the compressive strength of concrete, presence of steel reinforcement, interfacial surface conditions, and application of axial load on the composite steel and

[1]Department of Civil, Architectural and Environmental Engineering, Missouri University of Science and Technology, Rolla, MO

Corresponding Author:
Mohamed A. ElGawady, elgawadym@mst.edu

concrete section or the steel section only were investigated. It was concluded that the shear bond strength depends on the interface roughness and compressive strength of concrete. Values up to 3.6 MPa (0.52 ksi) were reported for the bond strength between smooth steel bars and confined normal strength concrete cylinders (*14*). The AISC (*15*) recommends a bond strength of 1.4 MPa [0.20 pounds per square inch (psi)] for hollow structural steel (HSS) having circular sections and 0.7 MPa (0.1 ksi) for HSS having rectangular sections. Axial loading on the steel piles does not change the bond strength.

Polymer concrete (PC) is a type of concrete–polymer composite, which generally has higher strength, higher resistance to chemicals and corrosive salts, lower water absorption, and higher freeze–thaw stability than CC (*16*, *17*). PC is used in infrastructure exposed to aggressive environmental conditions and has been used successfully in bridge decks, crack repairs, machine foundations, and precast façade panels as well as wastewater and potable water pipes (*18*, *19*). Different types of resins such as epoxy, polyester, and methyl methacrylate (MMA) have been used as the polymer in PC.

Methyl methacrylate polymer concrete (MMA-PC) has been investigated in this study. The MMA is a type of PC that has been used for many years as industrial flooring with satisfactory performance, and has provided excellent workability during placement and rapid curing time. It is also designed for use in new construction and rehabilitation of bridge decks, expansion joints, bearing pads, and other concrete structures. Only one study has been conducted to investigate the bond strength of the polymethyl methacrylate PC (PMMA-PC) with steel elements and reported a high bond performance with deformed steel rebars ranging from 25.3 to 36.7 MPa (3.6 to 5.3 ksi) (*20*). To date, there is no research investigating the bond strength of MMA-PC.

Research Significance

Although there has been some research on structural applications of PC (*21–24*), research on the bond behavior of PC is limited. That limited research displayed the superior bond strength of PMMA-PC with deformed rebar. Therefore, MMA-PC has the potential to be a solution for encasing corroded steel H-piles if the bond between the MMA-PC and H-piles is quantified. This paper presents the experimental results of push-out tests of seven steel H-piles encased in concrete jackets. Six of the steel piles were encased in MMA-PC jackets and the seventh steel pile was encased in CC. Two different jacket configurations and three different embedment lengths were used for the MMA-PC specimens. The MMA-PC bond-slip curves of the test specimens are presented for the first time as well. The main objective of this paper is to determine the bond stress-slip of MMA-PC and CC encasing H-piles.

Experimental Program

Test Program

Seven specimens were tested using the push-out method to examine the bond strength for different concrete encasements (Table 1). The MMA-PC jackets were placed into three different embedment lengths, L_e, of 63.5 mm (2.5 in.), 127 mm (5.0 in.), and 190.5 mm (7.5 in.) (Figure 1), and the CC jacket had a L_e of 254 mm (10 in.). The specimens' designations include four components: (1) the concrete mix type, PC or CC, (2) the jacket cross-section configuration (P-prism or C-cylindrical), (3) design concrete compressive strength in ksi, and (4) the L_e value as multipliers of 63.5 mm (2.5 in.) [e.g., 2 = 127 mm (5.0 in.)].

Material Properties

Steel H-Pile. Three steel coupons were cut from each of the flange and web parts of the steel H-pile to determine their mechanical properties (Table 2). The steel coupons were tested in tension per ASTM E8/E8M – 16a (*25*) with strains in the middle region measured using 25.4 mm (1.0 in.) long clip gage.

Table 1. Parametric Study

Group	Specimen code	Concrete type	f'_c MPa (ksi)	Concrete jacket length, L_e mm (in.)
A	PC-P-9-1	Methyl methacrylate polymer concrete (MMA-PC)	63.0 (9.2) ± 0.2	63.5 (2.5)
	PC-P-9-2			127.0 (5.0)
	PC-P-9-3			190.5 (7.5)
B	PC-C-9-1			63.5 (2.5)
	PC-C-9-2			127.0 (5.0)
	PC-C-9-3			190.5 (7.5)
C	CC-C-9-4	Conventional concrete (CC)	65.5 (9.5) ± 0.1	254.0 (10)

Note: ksi = kips per square inch.

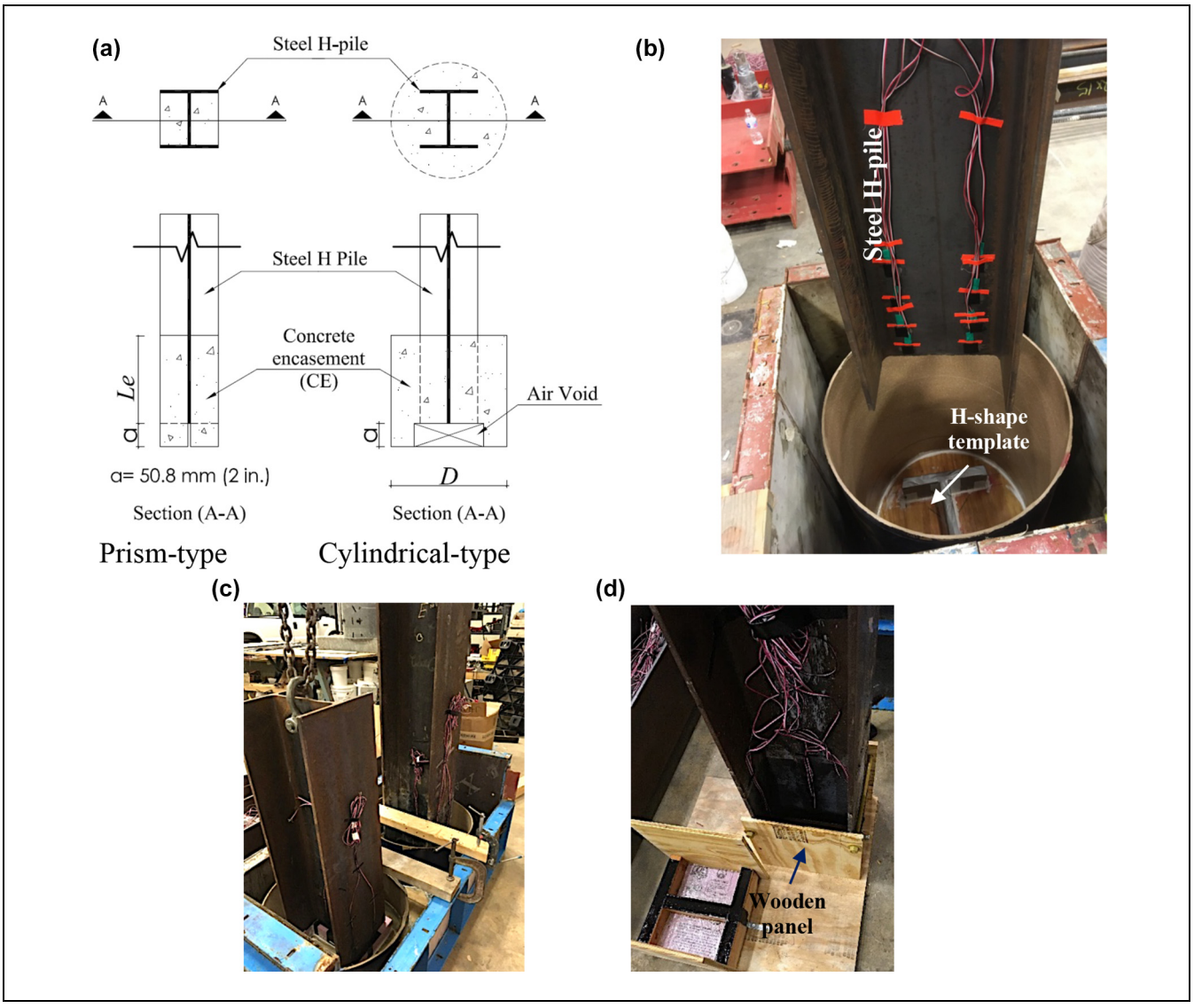

Figure 1. Specimen preparation: (*a*) layout, (*b*) placing the pile on the formed template, (*c*) pile placed inside the cardboard, and (*d*) pile placed inside a wooden box form.

Table 2. Mechanical Properties of the Steel H-Pile

Section	Yield stress MPa (ksi)	Ultimate stress MPa (ksi)	Elastic modulus GPa (10^3 ksi)	Rupture strain (ε_u, in./in.)
Flange	324 (47)	517 (75)	181 (26.25)	0.100
Web	407 (59)	503 (73)	182 (26.40)	0.125

Note: ksi = kips per square inch.

Polymer Concrete. Commercially available prepackaged MMA-PC, T-17, was used. The T-17 consists of two components: resin and hardener. The resin consists of a solvent-free 100% reactive, low-viscosity MMA. The characteristics of MMA include excellent transparency, strong weather resistance, and good colorability. The hardener consists of a blend of sand, inert fillers, polymers, and initiators. Coarse aggregate with sizes ranging from 19 to 9.5 mm (0.75 to 0.375 in.) was used with the T-17 mixtures. The mix design followed the

Table 3. Specimen Geometrical Properties

Steel H-pile	Concrete encasement		
Section	Configuration	Contact perimeter (p) mm (in.)	Diameter (D) mm (in.)
250 × 62 (10 × 42)	Cylinder Prism	1,498.6 (59.0) 942.3 (37.1)	508 (20)

recommendations of the manufacturer. The 3-day compressive strength, f'_c, of MMA-PC, was 63.4 MPa (9.2 ksi) (*26*) and the tensile strength was 12.5 MPa (1.8 ksi) (*27*).

Preparation of Test Specimens. Table 3 and Figure 1*a* present the steel H-piles and concrete jackets used. For the specimens with cylindrical jackets, a steel H-pile is placed inside cardboard having a diameter (D) of 508 mm (20 in.) (Figure 1*b, c*). For the specimens with prismatic jackets, a steel H-pile is placed inside a wooden plate form fixed to the H-pile flanges (Figure 1*d*).

A steel H-pile was inserted into the formwork and was fitted on top of an H-shaped 50.8 mm (2 in.) high formed template (Figure 1*b, c*). The H-shaped template was used to form a gap inside the concrete jacket underneath the steel H-pile specimen (Figure 1*a*), which allowed the steel H-pile to slip downward freely.

Concrete Encasement Casting and Curing

Mixing the CC followed ASTM C192-16 (*28*), and the MMA-PC mixture design and procedure followed the recommendations of the MMA-PC's supplier. A rotary drill mixer was used for mixing the MMA-PC components inside a big plastic bucket (Figure 2). The required amount of T-17 resin was poured into a plastic bucket, and then the T-17 powder component was added and mixed until it displayed a homogeneous appearance. The required coarse aggregate was added and re-mixed for another minute.

For the CC concrete encasement, the cardboard was demolded 2 days after placing the concrete jacket. Then, the concrete was covered with wet burlap sheets and cured at an ambient temperature of 23 ± 2°C (73 ± 3°F) until the testing day. Numerous 102 mm × 204 mm (4-in. × 8-in.) concrete cylinders were placed and exposed to the same ambient curing regime and were tested periodically during the curing period. Once the target compressive strength was reached, the curing was stopped, and the repaired specimens were tested.

Test Set-Up and Instrumentation

Electrical strain gauges were mounted on the steel H-piles before placing the concrete jacket, to measure the axial strain distributions during the test (Figure 3*a*). The strain gauges were arranged along different cross-sections 63 mm (2.5 in.) apart on average, and the first section located 31.75 mm (1.25 in.) from the free edge of the pile and extended along the embedded length of each jacket. Seven strain gauges were distributed at each horizontal cross-section (Figure 3*a* and *b*). The slip between the concrete jacket and steel was measured also using two linear variable displacement transducers (LVDTs) that were placed vertically, at 76.2 mm (3.0 in.) gauge length, on the flanges or webs of the steel piles in the case of cylindrical and prismatic jackets, respectively (Figure 3*c* and *d*).

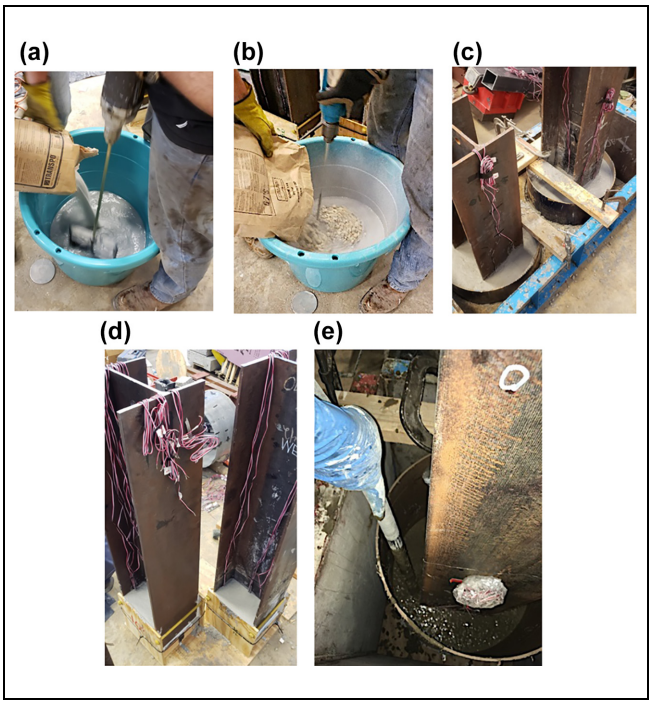

Figure 2. Concrete encasement placing: (*a*) placing the hardener and resin, (*b*) adding the aggregate, (*c* and *d*) placing the MMA-PC concrete in cylindrical and prismatic shapes, and (e) placing and vibrating the conventional concrete (CC).
Note: MMA-PC = methyl methacrylate polymer concrete; CC = conventional concrete.

Push-Out Test

The test specimens were tested by 2,500 kN (550 kips) MTS universal testing machine (Figure 4). The axially compressive force was monotonically applied on the top of the steel pile, in displacement control with a rate of 1.27 mm/min (0.05 in./min), using the MTS swivel plate, while the bottom of the concrete jacket was supported on a rigid steel base.

Results and Discussion

The push-out test results are summarized in Table 4. The average bond stress (τ) is defined using Equation 1 as the

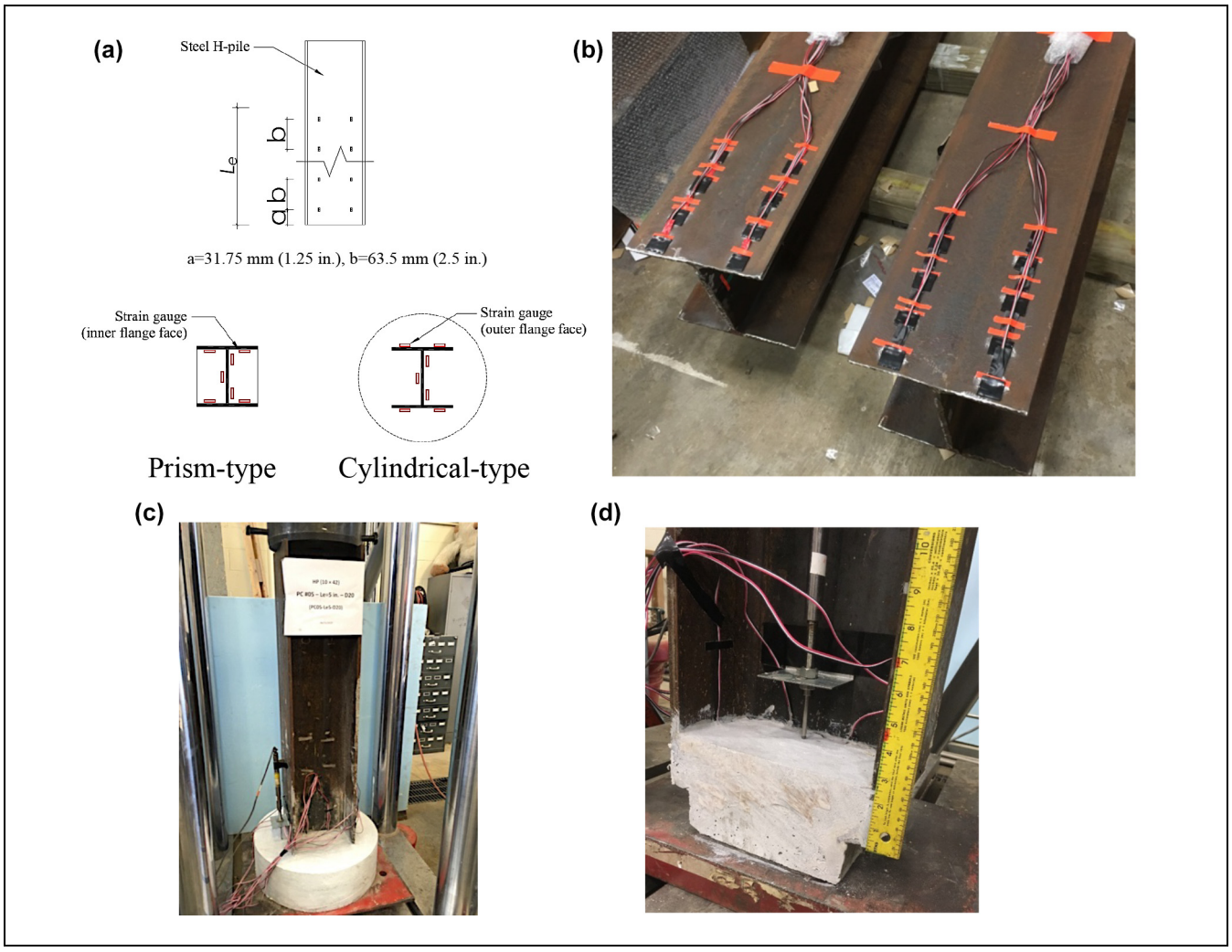

Figure 3. Instrumentation of the test specimens: (*a*) strain gauges distribution, (*b*) strain gauges mounted on the steel H-pile, (*c*) LVDTs mounted on the flanges of a steel pile with cylindrical jacket, and (*d*) LVDTs mounted on the webs of a steel pile with prismatic jacket.
Note: LVDT = linear variable displacement transducers.

axial load normalized by the contact area between the concrete jacket and steel pile.

$$\tau = \frac{F}{pL_e} \tag{1}$$

where F is the applied axial load at the free loaded end, p is the perimeter of the H-pile cross-section that is in contact with concrete jacket = 1,498.6 mm (59.0 in.) for cylindrical configuration, 942.3 mm (37.1 in.) for prism configuration, and L_e is the steel pile embedded length (Table 4). Equation 1 assumes uniform bond stress distribution along the embedment length of the steel pile.

The relative slip between the steel H-pile and the concrete jacket at the loaded end was obtained from the LVDT readings that attached to the steel H-pile web and flanges (Figure 4*a*). These slip calculations ignore the axial deformation in the steel pile specimen, which can be justified given the short gauge length of the LVDT and the low stresses in the steel sections inside the concrete jacket.

Failure Modes

Figure 5 shows the failure modes of the tested specimens. Generally, failure occurred at the concrete jacket–steel section interface along the jacket length while sliding against each other.

For the prism-type encased specimens, failure initiated at a minimal slip of the jacket followed by an abrupt bond-breaking at the ultimate load without any evidence of concrete splitting cracks (Figure 5*a* and *b*). After that, a sharp decrease in the load-carrying capacity occurred as the slip increased. Furthermore, the cylindrical-type

Table 4. Results of the Push-Out Tests

Concrete type	Specimen ID and jacket shape		L_e mm (inch)	Peak load (P) kN (kips)	Maximum bond stress (τ_{max}) MPa (ksi)	Slip (δ)* mm (inch $\times 10^{-2}$)
MMA-PC	PC-P-9-1	**Prism**	63.5 (2.5)	200 (44.7)	3.31 (0.48)	0.068 (0.27)
	PC-P-9-2		127.0 (5.0)	345 (77.0)	2.96 (0.43)	0.071 (0.28)
	PC-P-9-3		190.5 (7.5)	722 (161.2)	4.06 (0.59)	0.104 (0.41)
	PC-C-9-1	**Cylindrical**	63.5 (2.5)	189 (42.2)	2.00 (0.29)	0.025 (0.10)
	PC-C-9-2		127.0 (5.0)	542 (121.0)	2.82 (0.41)	0.107 (0.42)
	PC-C-9-3		190.5 (7.5)	845 (188.5)	2.90 (0.42)	0.091 (0.36)
CC	CC-C-9-4		254.0 (10)	317 (70.8)	0.83 (0.12)	0.028 (0.11)

Note: *At the peak load. MMA-PC = methyl methacrylate polymer concrete; CC = conventional concrete; ksi = kips per square inch.

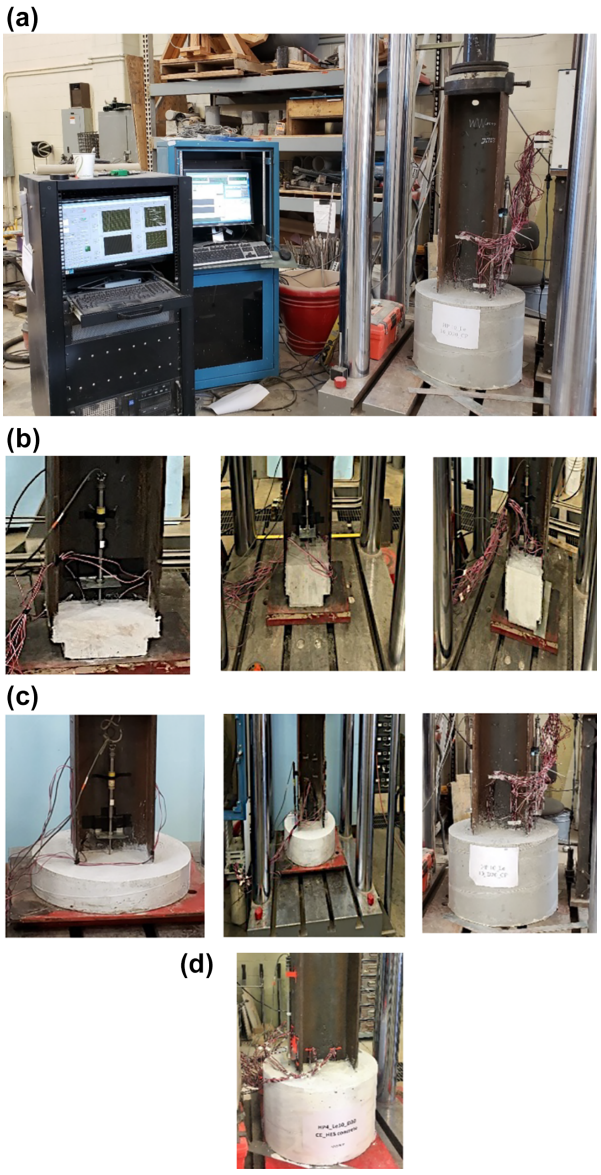

Figure 4. Concrete-encased steel H-piles: (*a*) test layout, (*b*) prism-type encased specimens, (*c*) cylindrical-type encased specimens, and (*d*) conventional concrete (CC) specimen.

MMA-PC-encased specimen displayed similar behavior with one exception. At the peak load, failure occurred because of splitting cracks that started at the flange tips as a result of the high tensile hoop stress concentrations. The cracks extended radially toward the perimeter of the jacket. Those cracks were formed and propagated very quickly (Figure 5*c* and *d*), leading to a significant decrease in the axial load capacity without any concrete crushing. Similar cracks propagated in the cylindrical-type CC specimen (Figure 5*e*); however, the propagation of the cracks was much slower than those developed in the MMA-PC specimens.

Bond Stress

Expectedly, the bond strength increased with an increase in the embedment length of the MMA-PC jacket (Table 4). Furthermore, except specimen PC-C-9-1, specimens having cylindrical-type MMA-PC jackets displayed a 17% larger peak load than those with the prism-type MMA-PC jackets at the same L_e of 190.5 mm (7.5 in.). This occurred as the interface surface area of the MMA-PC–steel pile in the case of the cylindrical-type jacket is 59% larger than that of the prism-type jacket. Furthermore, all MMA-PC specimens that had an embedment length of 127 mm (5 in.) or more displayed bond forces ranging from 8.1% (prism-type) to 41.5% (cylindrical-type) higher than that of the CC having an embedment length of 254 mm (10 in.). The encasement using MMA-PC with an embedment length of 190.5 mm (7.5 in.) was able to develop 25% and 30% of the squash load of the investigated pile in the case of prism and cylindrical types, respectively.

Figure 6*a* shows the bond strength τ_{max}, of the test specimens, and Figure 6*b* shows τ_{max} versus the L_e. As shown in the figure, the τ_{max} ranged from 4.06 MPa (0.59 ksi) to 0.83 MPa (0.12 ksi) with the CC displaying the lowest value of τ_{max}. The MMA-PC specimens displayed τ_{max} ranged from 258.3% to 391.7% that of the CC specimen. The τ_{max} values of the prism-type encased specimens were consistently higher than or equal to those

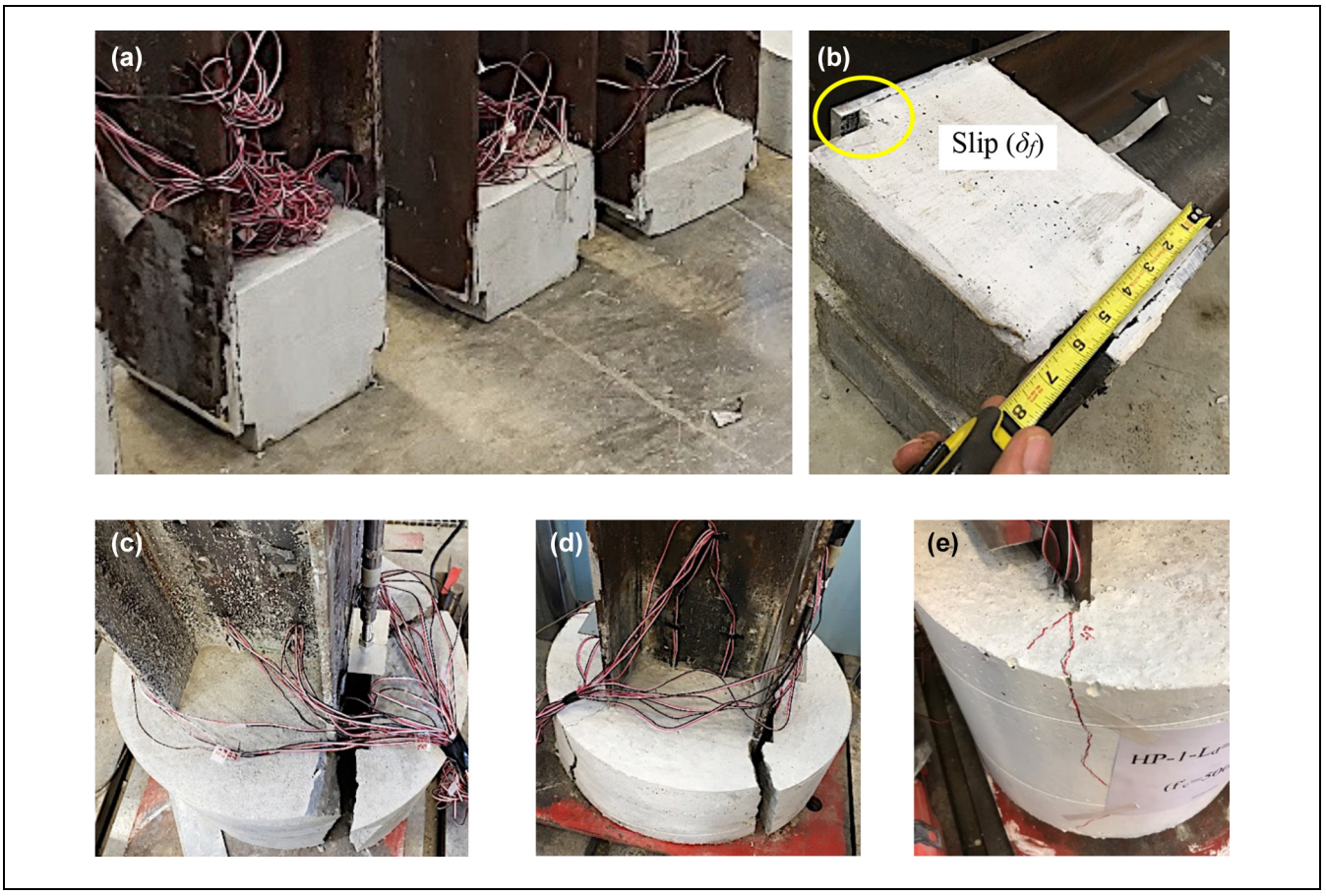

Figure 5. Modes of failure of (*a, b*) MMA-PC tested specimens, (*c, d*) MMA-PC cylindrical-type specimens, and (*e*) CC specimen.
Note: MMA-PC = methyl methacrylate polymer concrete; CC = conventional concrete.

of the cylindrical-type specimens. The τ_{max} of the prism-type specimens does not correlate well with the L_e and ranged from 2.96 MPa (0.43 ksi) to 4.06 MPa (0.59 ksi) (Table 4 and Figure 6*b*). Therefore, for the design of prism-type jackets for steel piles, a τ value of 2.96 MPa (0.43 ksi) represents a reasonable assumption. For the cylindrical-type jackets using MMA-PC, τ_{max} ranged from 2 MPa (0.29 ksi) to 2.9 MPa (0.42 ksi) (Table 4). The value of τ_{max} increased with an increase in the value of L_e from 63.5 mm (2.5 in.) to 127 mm (5 in.); beyond that with increasing the value of the L_e the value of τ_{max} reached its threshold at a value of 2.9 MPa (0.42 ksi) (Table 4 and Figure 6*b*). Therefore, for the design of cylindrical-type jackets for steel piles, a τ value of 2 MPa (0.29 ksi) represents a reasonable assumption.

Figure 6*c* illustrates the embedded length versus the bond strength ($\tau_{max}p$) of the tested specimens normalized by $\sqrt{f'_c}$ to eliminate the influence of the variation in the strength of the two different types of concrete being 63.0 MPa (9.2 ksi) and 65.5 MPa (9.5 ksi) for the CC and PC, respectively. As shown in the figure, the normalized bond strength $\left(\tau_{max}p/\sqrt{f'_c}\right)$ for the PC ranged from 7.2 to 8.0 depending on the embedment length and encasement type. For the CC specimen, the $(\tau_{max}p/\sqrt{f'_c})$ was 2.2 (in. $\sqrt{}$psi), that is, ranging from 69.4% to 72.5% less than that of the PC prism- and cylindrical-type specimens (Figure 6*c*).

Figure 6*a* and *b* also shows the concrete/steel shear bond strength values of 1.4 MPa (0.20 psi) and 0.7 MPa (0.1 ksi) recommended by the AISC (2010) for concrete-filled HSS having circular and rectangular cross-sections. As shown in the figure, the AISC (2010)'s recommended value for HSS having a rectangular cross-section represents a lower bound for all test specimens. For the CC specimen, the measured shear bond stress exceeded those recommended by the AISC (2010) for concrete-filled HSS having rectangular cross-sections by 20%. However, the recommended AISC value for rectangular and circular HSS sections represents only 17–34% of the maximum bond strength measured for a specimen having a prism-type MMA-PC jacket, and it represents only 24–47% of the maximum bond strength measured for a specimen having a cylindrical-type jacket, respectively.

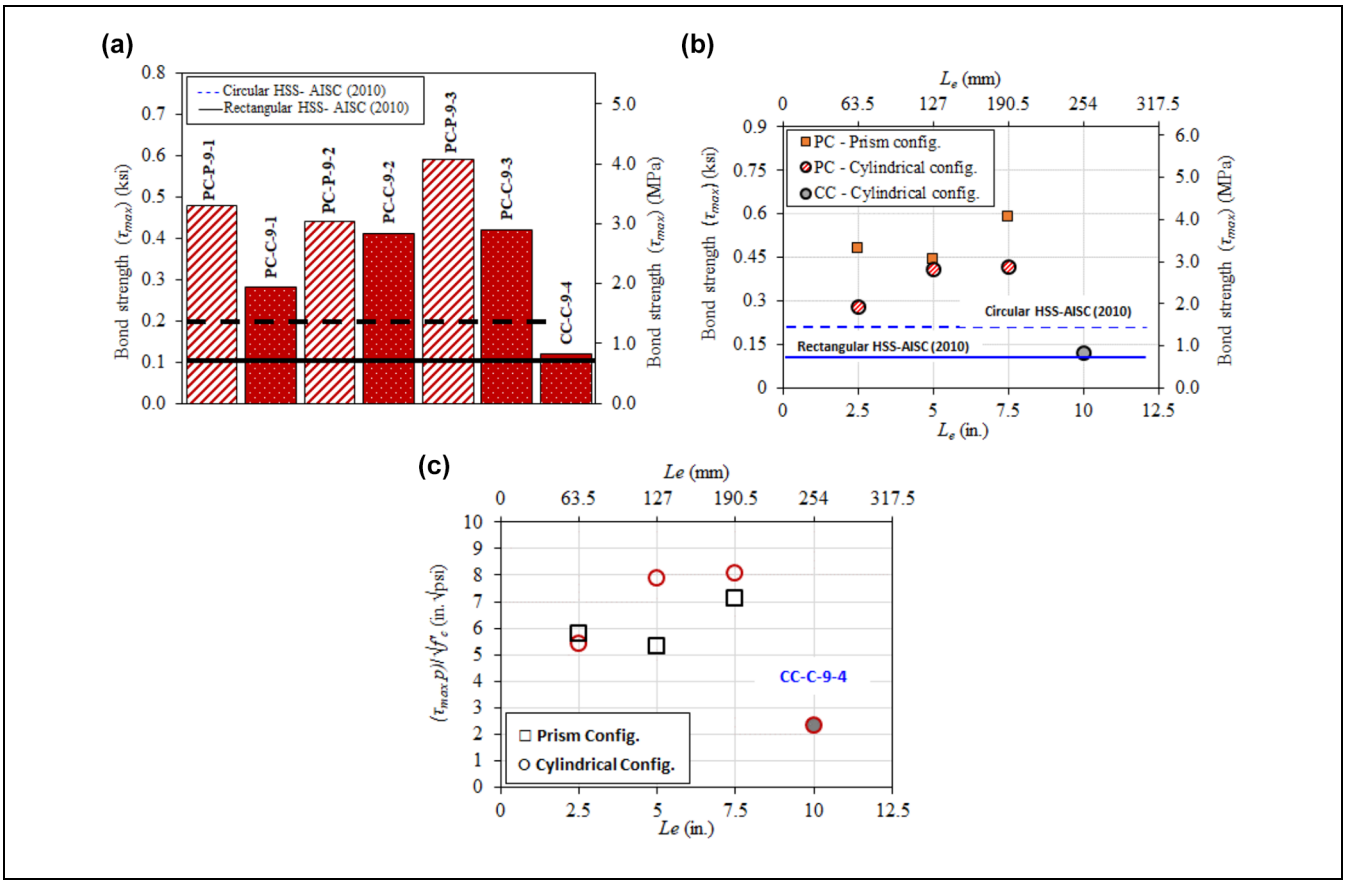

Figure 6. Bond strength values, τ_{max}: (*a*) of the tested specimens, (*b*) versus the embedment length, and (*c*) normalized by ($p/\sqrt{f'_c}$) versus the embedded length.

Bond Stress-Slip Curves

Three intercorrelated mechanisms control the general mechanics of stress transfer by the bond between steel elements embedded in concrete: (a) concrete chemical adhesion, (b) friction between the steel element and concrete, and (c) mechanical interlocking offered by the deformation of the interface surface roughness (*29–32*). In this study, the surface of the steel H-pile was quite smooth; thus, mechanical interlocking was minimal, and only chemical adhesion and friction were considered.

Figure 7*a* shows a schematic of the obtained bond stress-slip (τ- δ) model curve for the tested specimens. A bilinear type model divided into an elastic linear ascending part and a plastic (debonding) descending part, was observed (Figure 7*a*). The maximum bond stress in the elastic part was defined as (τ_{max}), with the relative displacement (slip) (δ_o) corresponding to τ_{max}. In the initial loading stage ($\delta < \delta_o$), the bond resistance is related mainly to the chemical adhesion. At δ_o and τ_{max}, failure initiated, and the failure mechanism depended on the type of the encasement. For cylindrical-type concrete-encased specimens, the tensile strength of the concrete jacket was unable to sustain the radial component of the splitting force, causing concrete cracking. For $\delta_o < \delta < \delta_f$, as the slip increased, the internal cracks propagated very rapidly in the case of MMA-PC and slowly in the case of CC at the smallest concrete jacket thickness near the tips of the flanges toward the concrete outer perimeter.

The same model holds for the prism-type concrete-encased specimens except that τ_{max} occurred just before bond failure between the encasement and steel H-pile. The plastic (debonding) descending part ended at δ_f and followed by either slight residual bond stress in the case of MMA-PC specimens with a prism-type encasement or zero bond stress in the case of MMA-PC specimens with cylindrical-type encasement (Figure 7*b–e*).

Conclusions

This paper investigates the bond behavior of concrete encasing steel H-piles. This encasement can be used to repair corroded H-piles in which the encasement bridges the applied load over the corroded section. Seven H-pile specimens encased in concrete jackets having different shape configurations, namely cylindrical and prism, as

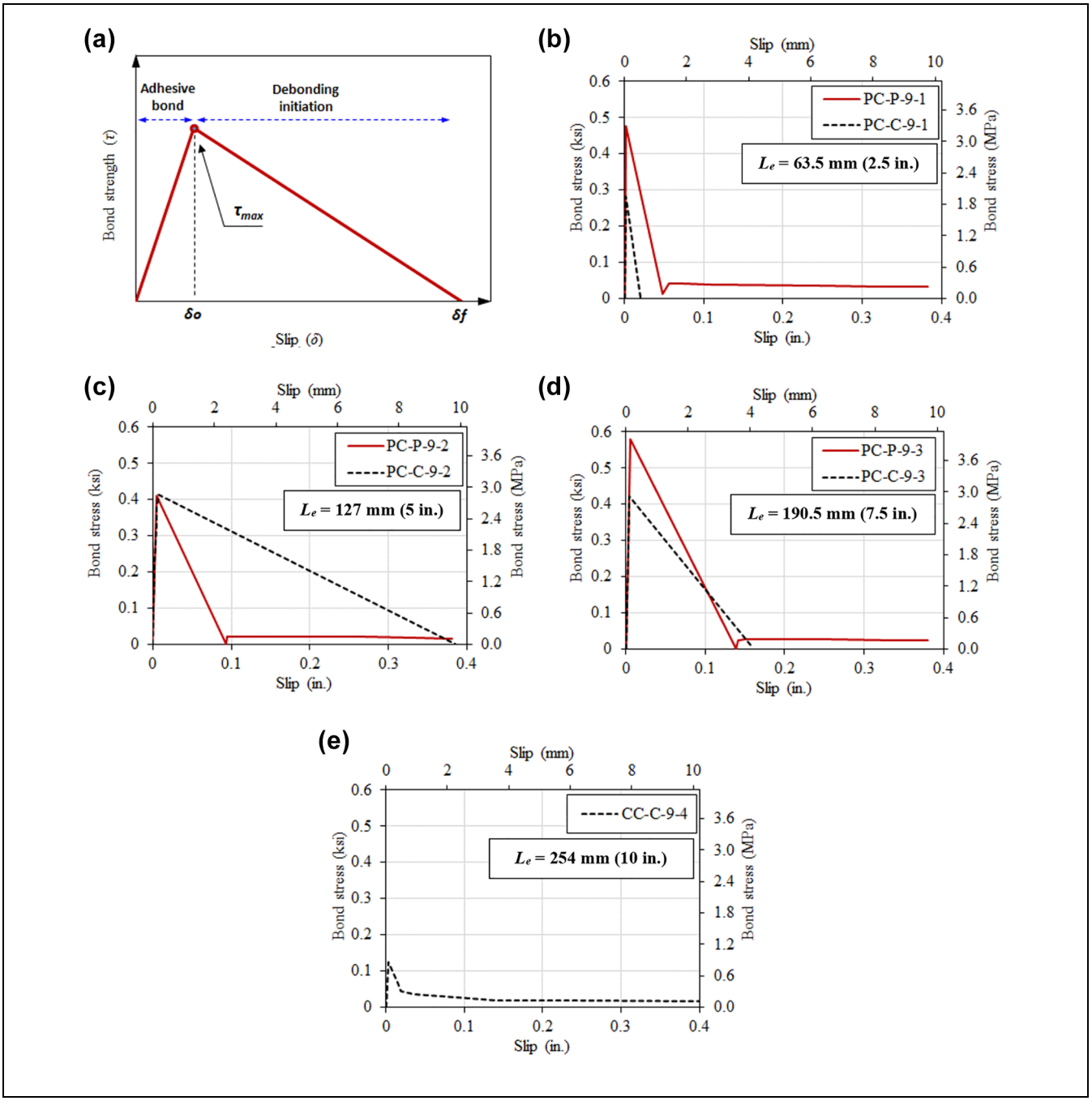

Figure 7. Typical bond strength (τ_{max}) versus slip model and bond stress versus slip curves of the tested specimens. (*a*) Bond-slip law, (*b-d*) MMA-PC specimens, and (e) CC specimen.
Note: MMA-PC = methyl methacrylate polymer concrete; CC = conventional concrete.

well as embedment lengths ranging from 254 mm (10 in.) to 63.5 mm (2.5 in.) were tested. Two different concrete types—ordinary Portland cement concrete (CC) and methyl methacrylate polymer concrete (MMA-PC)—were used to cast the encasements. The bond strengths between the concrete and piles were tested using push-out tests. The experimental work revealed the following conclusions:

1. The load-carrying capacity of the MMA-PC encasement is generally higher than that of the CC encasement. Specimens encased in MMA-PC with embedment lengths of 127 mm (5 in.) and 190.5 mm (7.5 in.x) reached up to 391.7% higher than that of the CC specimen having an embedment length of 254 mm (10 in.). Such significant improvement in the bond strength can allow a

significant reduction in the required encasement jackets for the repair of steel H-piles.
2. Piles encased in the cylindrical-type jackets displayed less shear bond stress compared with those encased in prism-type jackets. However, as the cylindrical jackets have larger interface contact surface with the steel piles, specimens having cylindrical jackets displayed higher forces than the corresponding specimens having prism jackets.
3. The AISC recommended value for the shear bond strength between concrete and HSS having rectangular cross-sections can be used to determine the shear bond strength between CC and steel piles. However, a shear bond stress of 2.96 MPa (0.43 ksi) can be used for the design of MMA-PC jackets having an embedment length of at least 127 mm (5 in.).
4. The bond-breaking for most of the tested specimens occurred at a minimal slip value of 0.051 mm (0.002 in.), which is found to be the point of the concrete encasement (CE) splitting initiation (bond-breaking).

Acknowledgments

The authors would like to thank Transpo®, Inc. for donating the polymer concrete materials. Appreciation is extended to Skyline Steel for donating the H-piles.

Author Contributions

The authors confirm contribution to the paper as follows: study conception and design of the experiment: M. ElGawady; data collection: M. Abdulazeez, and Kyle Brown; analysis and interpretation of results: M. Abdulazeez and M. ElGawady; draft manuscript preparation: M. Abdulazeez; editing and reviewing the manuscript: M. ElGawady. All authors reviewed the results and approved the final version of the manuscript.

Declaration of Conflicting Interests

The author(s) declared no potential conflicts of interest with respect to the research, authorship, and/or publication of this article.

Funding

The author(s) disclosed receipt of the following financial support for the research, authorship, and/or publication of this article: The work in this research project was partially funded by the Missouri Department of Transportation (MoDOT).

References

1. Karagah, H., C. Shi, M. Dawood, and A. Belarbi. Experimental Investigation of Short Steel Columns with Localized Corrosion. *Thin-Walled Structures*, Vol. 87, 2015, pp. 191–199.
2. Shi, C., H. Karagah, M. Dawood, and A. Belarbi. Numerical Investigation of H-Shaped Short Steel Piles with Localized Severe Corrosion. *Engineering Structures*, Vol. 73, 2014, pp. 114–124.
3. Iskander, M. G., and A. Stachula. Wave Equation Analyses of Fiber-Reinforced Polymer Composite Piling. *Journal of Composites for Construction*, Vol. 6, No. 2, 2002, pp. 88–96.
4. Ramadan, A., and M. A. ElGawady. Axial Behavior of Corroded H-Piles. *Proc., IABSE Congress*, New York City, NY, 2019.
5. Ehsani, M. FRP Super Laminates Present Unparalleled Solutions to Old Problems. *Reinforced Plastics*, Vol. 53, No. 6, 2009, pp. 40–45.
6. Karagah, H., M. Dawood, and A. Belarbi. Experimental Study of Full-Scale Corroded Steel Bridge Piles Repaired Underwater with Grout-Filled Fiber-Reinforced Polymer Jackets. *Journal of Composites for Construction*, Vol. 22, No. 3, 2018, p. 04018008.
7. Abdulazeez, M., B. Sherstha, and M. A. ElGawady. Retrofit of Corroded Steel H-Piles Using Concrete Encased in CFRP. *Proc., 10th New York City Bridge Conference*, New York City, NY, 2019.
8. Ramadan, A., and M. A. ElGawady. Axial Behavior of Concrete Filled Pultruded FRP Box. *Proc., 1st Joint International Conference on Design and Construction of Smart City Components*, Cairo, Egypt, 2019.
9. Wan, B., C. M. Foley, S. W. Ainge, and C. Nguyen. *Procedures, Cost and Effectiveness for Deteriorated Bridge Substructure Repair*. WisDOT ID No. 0092-11-08. Wisconsin Highway Research Program, Wisconsin Department of Transportation, 2013.
10. Soliman, K., A. Arafa, and T. M. Elrakib. Review of Design Codes of Concrete Encased Steel Short Columns Under Axial Compression. *HBRC Journal*, Vol. 9, No. 2, 2013, pp. 134–143.
11. Abdulazeez, M., B. Sherstha, E. Gomaa, A. Ramadan, and M. A. ElGawady. Bond Behavior of Steel Bridge H-Pile Columns Encased in Concrete Jackets. Transportation Research Board, Washington, D.C., 2019.
12. Pecce, M., and F. Ceroni. Bond Tests of Partially Encased Composite Columns. *Advanced Steel Construction*, Vol. 6, No. 4, 2010, pp. 1001–1018.
13. Grzeszykowski, B., and E. Szmigiera. Ductility Assessment of Two-Chord Composite Steel-Concrete Battened Columns. *Structure and Infrastructure Engineering*, Vol. 13, No. 11, 2017, pp. 1414–1424.
14. Liu, X., A. Nanni, and P. F. Silva. Rehabilitation of Compression Steel Members Using FRP Pipes Filled with Non-Expansive and Expansive Light-Weight Concrete. *Advances in Structural Engineering*, Vol. 8, No. 2, 2005, pp. 129–142.
15. AISC Committee. *Specification for Structural Steel Buildings*. ANSI/AISC 360-10. *American Institute of Steel Construction, Chicago-Illinois*, 2010.
16. Chandra, S., and Y. Ohama. *Polymers in Concrete*. CRC Press, Boca Raton, FL, 1994.
17. Mehta, P. K., and P. J. Monteiro. *Concrete Microstructure, Properties and Materials*. McGraw-Hill Education, New York, 2017.

18. Ferdous, W., A. Manalo, T. Aravinthan, and G. Van Erp. Properties of Epoxy Polymer Concrete Matrix: Effect of Resin-to-Filler Ratio and Determination of Optimal Mix for Composite Railway Sleepers. *Construction and Building Materials*, Vol. 124, 2016, pp. 287–300.
19. Emiroglu, M., A. E. Douba, R. A. Tarefder, U. F. Kandil, and M. R. Taha. New Polymer Concrete with Superior Ductility and Fracture Toughness Using Alumina Nanoparticles. *Journal of Materials in Civil Engineering*, Vol. 29, No. 8, 2017, p. 04017069.
20. Cao, X., and L. J. Lee. Control of Shrinkage and Final Conversion of Vinyl Ester Resins Cured in Low-Temperature Molding Processes. *Journal of Applied Polymer Science*, Vol. 90, No. 6, 2003, pp. 1486–1496.
21. Mantawy, I., R. Chennareddy, M. Genedy, and M. R. Taha. Polymer Concrete for Bridge Deck Closure Joints in Accelerated Bridge Construction. *Infrastructures*, Vol. 4, No. 2, 2019, p. 31.
22. Cervo, N. M., and A. J. Schokker. *Bridge Deck Patching Materials*. FHWA-PA-2007-023-510401-10. Pennsylvania Department of Transportation, 2008.
23. Alice, S. E. *Selection of High Performance Repair Materials for Pavements and Bridge Decks*. Cleveland State University, 2014.
24. ElBatanouny, M. K., E. I. Nadelman, J. C. Kurth, and P. SE. *Use of Polymer Overlays or Sealers on New Bridges*. The Iowa Highway Research Board, 2017.
25. ASTM, E8/E8M-13. *Standard Test Methods for Tension Testing of Metallic Materials*. ASTM International, West Conshohocken, PA, 2013.
26. ASTM, C579-18. *Standard Test Methods for Compressive Strength of Chemical-Resistant Mortars, Grouts, Monolithic Surfacings, and Polymer Concretes*. ASTM International, West Conshohocken, PA, 2018.
27. ASTM, D790-17. *Standard Test Methods for Flexural Properties of Unreinforced and Reinforced Plastics and Electrical Insulating Materials*. ASTM International, West Conshohocken, PA, 2017.
28. ASTM, C192/C192M-16. *Standard Practice for Making and Curing Concrete Test Specimens in the Laboratory*. ASTM International, West Conshohocken, PA, 2016.
29. du Béton, F. I. Bond of Reinforcement in Concrete: State-of-Art Report. *Bulletin*, Vol. 10, 2000, pp. 160–167.
30. Raynor, D. J., D. E. Lehman, and J. F. Stanton. Bond-Slip Response of Reinforcing Bars Grouted in Ducts. *Structural Journal*, Vol. 99, No. 5, 2002, pp. 568–576.
31. Hadi, M. N. Bond of High Strength Concrete with High Strength Reinforcing Steel. *The Open Civil Engineering Journal*, Vol. 2, 2008, pp. 143–147.
32. Harajli, M. Bond Stress–Slip Model for Steel Bars in Unconfined or Steel, FRC, or FRP Confined Concrete Under Cyclic Loading. *Journal of Structural Engineering*, Vol. 135, No. 5, 2009, pp. 509–518.